

- 5475 (1991); R. Taylor *et al.*, *Chem. Commun.* **1992**, 665 (1992); A. A. Tuinman *et al.*, *J. Phys. Chem.* **96**, 7584 (1992); I. Belaiish *et al.*, *Adv. Mater.* **4**, 411 (1992); T. Nakajima and Y. Matsuo, *Carbon* **30**, 1119 (1992); P. J. Benning *et al.*, *Phys. Rev. B* **47**, 1589 (1993); A. A. Tuinman *et al.*, *J. Am. Chem. Soc.* **115**, 5885 (1993); K. Kniaz *et al.*, *ibid.*, p. 6060.
3. R. F. Curl and R. E. Smalley, *Sci. Am.*, 62 (October 1991).
4. R. Taylor *et al.*, *Nature* **355**, 27 (1992).
5. These spheroidal molecules can be thought of as nanospheres covalently bonded to small oligomers of tetrafluoroethylene, the principal component of Teflon (a registered trademark for fluoropolymer resins, films, and fibers made by DuPont).
6. P. J. Krusic *et al.*, *J. Am. Chem. Soc.* **113**, 6274 (1991); P. J. Krusic, E. Wasserman, P. N. Keizer, J. R. Morton, K. F. Preston, *Science* **254**, 1183 (1991); J. R. Morton *et al.*, *J. Phys. Chem.* **96**, 3576 (1992); J. R. Morton *et al.*, *J. Chem. Soc. Perkin Trans. 2* **1992**, 1425 (1992); P. J. Krusic *et al.*, *J. Phys. Chem.* **97**, 1736 (1993); J. R. Morton *et al.*, *Chem. Phys. Lett.* **204**, 481 (1993); P. N. Keizer *et al.*, *J. Chem. Soc. Perkin Trans. 2* **1993**, 1041 (1993).
7. J. R. Morton *et al.*, *J. Am. Chem. Soc.* **114**, 5454 (1992).
8. Heating C₆₀ (300 mg) in a sealed vessel with perfluorohexyl iodide (6 ml) in 1,2,4-trichlorobenzene (15 ml) for 24 hours at 175°C under 5 to 20 psi of nitrogen produced dark red-brown reaction mixtures. The characteristic color of iodine vapor could be seen in the glass vessel during reaction. The residue obtained after removal of the solvent by distillation (10⁻⁴ torr) was highly soluble in hexafluorobenzene and CClF₂CCl₂F (Freon 113), in sharp contrast with the total insolubility of C₆₀ in these solvents, and was filtered from any remaining solids. It was purified by two precipitations from Freon 113 solutions with dichloromethane to yield a glassy solid when dried (1.35 g). A typical elemental analysis yielded an average formulation corresponding to C₆₀[(CF₂)₅CF₃]_{9.5}H₂ with traces of chlorine and no iodine (<100 ppm) in the sample (C, 36.85; H, 0.07; F, 61.66; and Cl, 0.50%). Traces of chlorine may arise from the solvent either during reaction or upon work-up. The ultraviolet-visible spectrum in Freon 113 showed a featureless, monotonically decreasing absorption in the range 200 to ~650 nm.
9. Argon was used as a buffer to reduce the kinetic energy of electrons to thermal levels.
10. Results of ¹⁹F NMR (283 MHz, 25°C, C₆F₆-CD₂Cl₂) : δ (in parts per million) = -81 (slightly broadened, 3F, CF₃); -96 to -111 [extremely broad, 2F, CF₂(α)]; -113 to -118 [broad, 2F, CF₂(β)]; -121 [broad, 2F, CF₂(γ)]; -122 [slightly broadened, 2F, CF₂(δ)]; and -126 [slightly broadened, 2F, CF₂(ε)]. The assignments refer to the position on the perfluoroalkyl chain: C₆₀-CF₂(α)-CF₂(β)-CF₂(γ)-CF₂(δ)-CF₂(ε)-CF₃. We assume that the further a CF₂ group is from the C₆₀ surface, the sharper the resonance of its fluorines will be. Resonances assigned to CF₂ groups closer to the surface are broad because the material is a mixture of different isomers. There is thus a variety of different local chemical environments for the diastereotopic fluorines of the CF₂ groups closer to the C₆₀ surface.
11. D. Griller *et al.*, *J. Am. Chem. Soc.* **103**, 7761 (1981).
12. C. Rüchardt *et al.*, *Angew. Chem. Int. Ed. Engl.* **32**, 584 (1993).
13. The expected product from this mechanism, α,α,α-trifluoro-toluene, was detected by ¹⁹F NMR and by gas chromatography-mass spectrometry together with smaller amounts of iodobenzene.
14. S. J. McLain, B. Sauer, L. Firment, *Polym. Prepr. Am. Chem. Soc. Div. Polym. Chem.* **34**, 666 (1993).
15. The equivalence of the two fluorines in the perfluoroethyl adduct can be attributed to the presence of a plane of symmetry and not to fast exchange between different environments because no line-shape effects were observed over a very broad temperature range.
16. In ESR, the activation energies that can be extracted from the analysis of temperature-dependent line-shape effects of the kind shown in Fig. 3A are generally less than ~5 kcal/mol.
17. See, for example, D. A. Dixon, *J. Phys. Chem.* **96**, 3698 (1992).
18. F. N. Tebbe *et al.*, *Science* **256**, 822 (1992).
19. With the use of standard Corey-Pauling-Koltun (CPK) models, a CF₃ group viewed along the threefold axis can be inscribed by a circle whose diameter is about 33% larger than the diameter of a bromine atom.
20. The structure shown in Fig. 3 is the result of a molecular mechanics calculation (Insight II Molecular Modeling Software; Biosym Technologies, Inc., San Diego, CA).
21. We thank K. Lykke for helpful contributions, D. Dixon for stimulating discussions, J. Krywko for molecular modeling, B. Sauer for contact-angle measurements, and S. Hill, R. Davis, J. B. Jensen, I. Kregers, and R. McKay for technical assistance. The FTMS work was carried out at the Argonne National Laboratory, Argonne, Illinois. DuPont contribution no. 6577.

24 May 1993; accepted 4 August 1993

Isotopic Evidence for Reduced Productivity in the Glacial Southern Ocean

A. Shemesh, S. A. Macko, C. D. Charles, G. H. Rau

Records of carbon and nitrogen isotopes in biogenic silica and carbon isotopes in planktonic foraminifera from deep-sea sediment cores from the Southern Ocean reveal that the primary production during the last glacial maximum was lower than Holocene productivity. These observations conflict with the hypothesis that the low atmospheric carbon dioxide concentrations were introduced by an increase in the efficiency of the high-latitude biological pump. Instead, different oceanic sectors may have had high glacial productivity, or alternative mechanisms that do not involve the biological pump must be considered as the primary cause of the low glacial atmospheric carbon dioxide concentrations.

Measurements of ancient air trapped in ice (1–3) indicate that global atmospheric CO₂ concentrations have changed greatly over the last 130,000 years. These concentrations during the last glacial period were lower by about 80 ppm than concentrations during the Holocene and last interglacial. There is agreement that oceanic processes were primarily responsible for these changes because the oceanic reservoir of CO₂ is about 60 times larger than that for the atmosphere (4). One general mechanism that helps to explain observed lower surface-ocean CO₂ concentrations is the enhanced photosynthetic uptake of CO₂ and subsequent removal of organic carbon to the deep ocean. This process is known as the biological pump (5). Scenarios to alter the efficiency of the biological pump involve changes in global phosphate extraction, denitrification, the C/P ratio of organic tissues, and the organic and inorganic sedimentary carbon pools. However, these scenarios fail to meet constraints placed by ocean sediments and polar ice records (6). The surface water in polar regions is critical for the control of the CO₂ system, because the deep sea interacts directly there with

the atmosphere. A series of models (7–9) demonstrated that atmospheric CO₂ concentrations could be lowered in concert with the biological consumption of nutrients in polar surface waters. Such decreases could be achieved by (i) an increase in high-latitude productivity, (ii) a decrease in the rate of exchange between deep oceanic and polar surface waters, or (iii) both.

This notion and consistent model results prompted an extensive search in the sedimentary record of the Southern Ocean for evidence of the predicted biogeochemical changes. Attempts to trace changes in surface nutrient concentration were made by the measurement of ¹³C and Cd/Ca ratios in planktonic foraminifera (10–11) and Ge/Si ratios in diatoms (12). Opal accumulation rates were used to estimate changes in paleoproductivity of the Southern Ocean (13, 14), and bulk sediment δ¹⁵N measurements were used to estimate changes in surface-water nitrate utilization (15). Although the results are somewhat in disagreement, none of the above studies support the scenario of high-latitude performed nutrients for the deglacial increase in atmospheric CO₂.

Here we tested further the hypothesized variability in the Southern Ocean biological pump over the last glacial cycle by analyzing organic matter preserved in diatom frustules. Diatoms are the main primary producers south of the present polar front, and therefore geochemical characteristics of the siliceous sediments of the Southern Ocean may provide a direct re-

A. Shemesh, Department of Environmental Sciences and Energy Research, Weizmann Institute of Science, Rehovot 76100 Israel.

S. A. Macko, Department of Environmental Sciences, University of Virginia, Charlottesville, VA 22903.

C. D. Charles, Scripps Institution of Oceanography, University of California, San Diego, La Jolla, CA 92093.

G. H. Rau, Institute of Marine Sciences, University of California, Santa Cruz, CA 95064.

flection of past surface-water chemistry and productivity. We compared glacial and Holocene organic material using the relative abundance of amino acids. Measurements of ^{13}C and ^{15}N of diatom organic matter [$\delta^{13}\text{C}_{\text{org}}$ and $\delta^{15}\text{N}$ (16)] were used to trace changes in productivity, nutrient utilization, and the dissolved carbonate system of the Southern Ocean. We used the $\delta^{13}\text{C}_{\text{org}}$ and $\delta^{13}\text{C}$ of planktonic foraminifera ($\delta^{13}\text{C}_{\text{pachy}}$) from the same core to evaluate surface-water CO_2 supply and biological demand.

Experimental and field observations (17, 18) strongly suggest that the concentration of dissolved molecular CO_2 , [$\text{CO}_{2(\text{aq})}$], is related to the $\delta^{13}\text{C}$ of the organic constituents of marine plankton. Such a relation presents the possibility that $\delta^{13}\text{C}$ values of plankton or their organic residues might serve as a proxy for surface-water [$\text{CO}_{2(\text{aq})}$] and, by inference, atmospheric CO_2 concentration (19). Although the general trend of the negative relation between [$\text{CO}_{2(\text{aq})}$] and $\delta^{13}\text{C}$ of organic matter has been observed, its exact magnitude depends on the photosynthetic carbon demand (20). Thus, at least three factors control the isotopic composition of marine organic matter: (i) the $\delta^{13}\text{C}$ of the inorganic carbon used as the substrate for photosynthesis, (ii) [$\text{CO}_{2(\text{aq})}$], and (iii) photosynthetic carbon demand, which should be directly related to primary production. Qualitatively, an increase in productivity or decrease in [$\text{CO}_{2(\text{aq})}$] will enrich the organic matter in ^{13}C (21). For the nitrogen isotopes, an enrichment of ^{15}N is expected in the organic material if the increased productivity is accompanied by higher NO_3^- utilization (22, 23). We used $\delta^{13}\text{C}$ analyses of the planktonic foraminifera *Neogloboquadrina pachyderma* (l.c.) shells (24) to provide an independent measure for the isotopic composition of the dissolved inorganic carbon system. These analyses were also used to represent, after correction for temperature and salinity, the isotopic composition of $\text{CO}_{2(\text{aq})}$ presumably used during photosynthesis. Therefore, in principle, changes in surface-water CO_2 and NO_3^- supply and demand can be reconstructed by measurements of down-core variations in $\delta^{13}\text{C}_{\text{org}}$, $\delta^{15}\text{N}$, and $\delta^{13}\text{C}_{\text{pachy}}$.

We separated and purified (25, 26) diatom samples from the piston cores RC13-271 (51°59'S 04°31'E; water depth of 3634 m) and RC13-256 (53°11'S 00°21'W; water depth of 3243 m) retrieved from the Atlantic sector of the Southern Ocean, south of the present polar front (27). The relative abundances of amino acids from RC13-271 (Fig. 1) are similar to those obtained from living diatom organic matter (28). The low carbon concentrations in the diatom opal (0.5%); its high glutamic acid, glycine, and alanine contents; and the amino acid similarity between $\text{HNO}_3\text{-HClO}_4\text{-}$

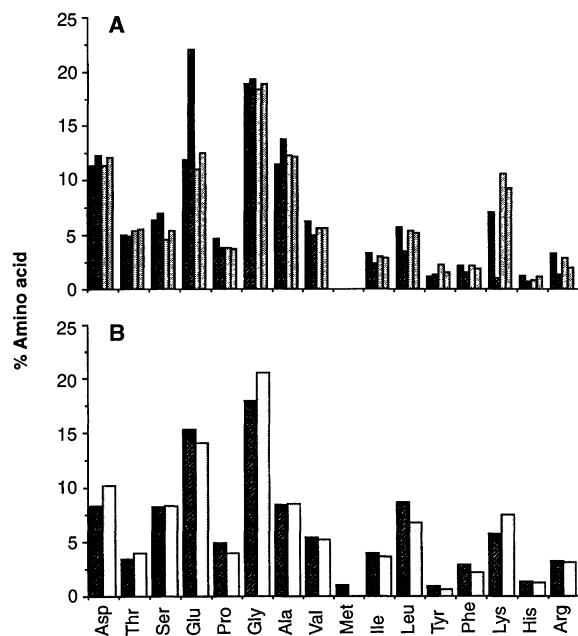


Fig. 1. (A) Percent soluble amino acids in two Holocene diatom samples (20 and 290 cm, cross-hatched bars) and in two Last Glacial Maximum (LGM) diatom samples (948 and 975 cm, shaded bars) from core RC13-271. (B) Comparison between percent amino acids of an untreated split (shaded bars) and an acid-treated split (cross-hatched bars) of a diatom sample from core RC13-271.

treated samples and untreated samples suggest that the organic material is a primary photosynthate associated with the organic matrix of biomineralization (29). The proteins are protected within the opal structure, which probably preserves their original composition through time. The amino acid patterns for glacial diatoms are nearly identical to those of the Holocene diatoms. This similarity enables the comparison between glacial and interglacial isotopic signals because it suggests that the organic material is not diagenetically altered or derived from different sources.

The down-core isotopic results (Figs. 2 and 3) show that $\delta^{13}\text{C}$ and $\delta^{15}\text{N}$ were the lowest during the Last Glacial Maximum

(LGM) and that ^{13}C and ^{15}N were depleted in diatom organic material during isotopic stage 2. The $\delta^{13}\text{C}_{\text{pachy}}$ results also exhibit a minimum during the LGM, although it lags the one in the $\delta^{13}\text{C}_{\text{org}}$ and $\delta^{15}\text{N}$ data. The difference between the Holocene and LGM values is 3.5 per mil in $\delta^{13}\text{C}_{\text{org}}$, 4.5 per mil in $\delta^{15}\text{N}$, and 1 per mil in $\delta^{13}\text{C}_{\text{pachy}}$. Both $\delta^{13}\text{C}_{\text{org}}$ and $\delta^{15}\text{N}$ values are in the range of the values for Southern Ocean sediments (15, 30). The observed glacial depletion in ^{13}C and ^{15}N argues against the possibility that primary production was higher during the glacial stage, because an isotopic enrichment of all three tracers is expected if glacial productivity was higher than the Holocene productivity. This conclusion is

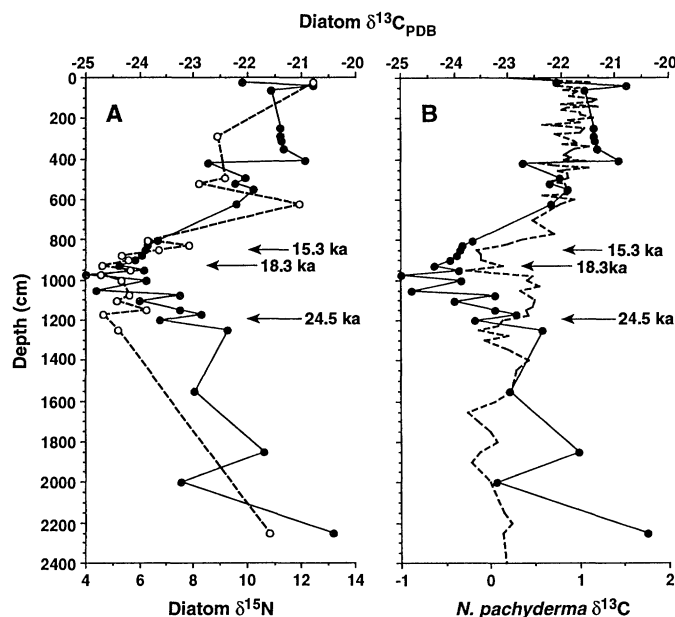


Fig. 2. Down-core variation in three isotopic tracers in core RC13-271. (A) Diatom $\delta^{13}\text{C}$ (solid trace) and diatom $\delta^{15}\text{N}$ (dashed trace). (B) Diatom $\delta^{13}\text{C}$ (solid trace) and *N. pachyderma* $\delta^{13}\text{C}$ (dashed trace); *N. pachyderma* ^{14}C ages at 850, 925, and 1200 cm (24) are indicated by arrows. All traces show an isotopic depletion during the maximum glacial stage.

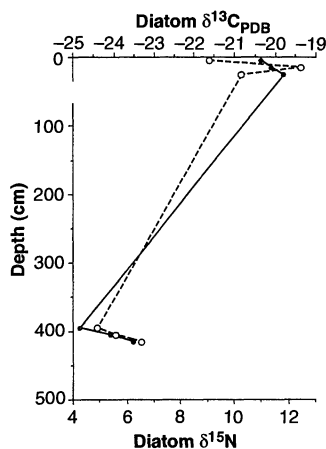


Fig. 3. Holocene-LGM variation in diatom $\delta^{13}\text{C}$ (solid trace) and $\delta^{15}\text{N}$ (dashed trace) in core RC13-256. Samples at the upper 50 cm represent the Holocene, whereas samples at around 400 cm represent the LGM according to radiolaria (*C. davisiana*) stratigraphy (34).

in accord with other studies that suggest that the productivity in the southern Atlantic was lower during the LGM (13, 14).

Part of the LGM ^{13}C depletion in the *N. pachyderma* record could be attributed to shifts in the zone of maximum gas exchange in the South Atlantic during the glacial period, an effect that has been invoked to reconcile the discrepancy between $\delta^{13}\text{C}_{pachy}$ and the nearly constant Cd/Ca ratios (24). Although this explanation can account for the $\delta^{13}\text{C}_{pachy}$ data, it requires that the same isotopic change be observed in the diatom organic matter, because productivity is held constant. Our records demonstrate that the isotopic change in the diatom $\delta^{13}\text{C}_{org}$ is three to four times that of the $\delta^{13}\text{C}_{pachy}$. Thus, an alternative mechanism is needed to satisfy the records of all three tracers.

Two independent processes can alter the carbon isotopic composition of organic matter and foraminifera to explain the observed LGM-Holocene differences. The first is a change in surface-water primary production. If marine algae use $\text{CO}_{2(aq)}$ for photosynthesis, the isotopic composition of the photosynthate depends on the ratio between intracellular and external $\text{CO}_{2(aq)}$, the $\delta^{13}\text{C}$ of ambient $\text{CO}_{2(aq)}$, the isotopic fractionation during CO_2 diffusion into the cell, and the isotopic fractionation associated with enzymatic CO_2 fixation (20, 21). On the basis of this model, an increase in productivity or carbon demand results in increased isotopic disequilibrium between ambient and intracellular $\text{CO}_{2(aq)}$; the net effect is to force a proportional increase in $\delta^{13}\text{C}_{org}$. Thus, the observed glacial ^{13}C depletion in diatom organic matter could indicate that productivity was lower during that time. Furthermore, the production of ^{13}C -depleted organic matter raises the $\delta^{13}\text{C}$

in the unused inorganic carbon pool. In high primary production regimes, $\delta^{13}\text{C}$ values of *N. pachyderma* (presumably reflecting the bicarbonate $\delta^{13}\text{C}$) are expected to be higher, whereas in low primary production regimes *N. pachyderma* $\delta^{13}\text{C}$ values are expected to be lower. Hence, the observed $\delta^{13}\text{C}_{pachy}$ record can be explained by reduced glacial productivity in surface waters.

The relation between $\delta^{15}\text{N}$ in organic material and NO_3^- utilization indicates that $\delta^{15}\text{N}$ values are high when NO_3^- utilization is high (22, 23). Thus, $\delta^{15}\text{N}$ values are higher with increasing primary production if the nutrient input remains constant in both concentration and isotopic composition. The low glacial $\delta^{15}\text{N}$ values indicate that NO_3^- utilization during this time was low, which may be attributed to reduced primary production if the supply of nutrients to the surface water was held constant in the region. Thus, all three isotopic records are consistent with reduced glacial primary productivity, but none of the observed isotopic trends can be explained by high productivity during the glacial stage. Further calibration of the isotopic tracers is needed to quantify the exact reduction in primary production.

The second process that alters the carbon isotopic composition of organic matter is a change in surface-water dissolved $[\text{CO}_{2(aq)}]$. The empirical relation between organic $\delta^{13}\text{C}$ and $[\text{CO}_{2(aq)}]$ suggests that $\delta^{13}\text{C}_{org}$ decreases approximately 0.6 per mil per 1 μM increase in $[\text{CO}_{2(aq)}]$ and that >85% of the global variation in $\delta^{13}\text{C}_{org}$ can be explained by changes in $[\text{CO}_{2(aq)}]$ (31). This relation suggests that the full magnitude of the low glacial $\delta^{13}\text{C}_{org}$ ratios can be accounted for by an increase of about 5 μM in surface-water $[\text{CO}_{2(aq)}]$ during the glacial stage. Such an increase coupled with the sea-surface temperature (26) would produce an ocean CO_2 partial pressure that would be out of equilibrium with LGM atmospheric CO_2 concentrations (2). However, a glacial $[\text{CO}_{2(aq)}]$ increase is not necessarily incompatible with lower global atmospheric values, because local disequilibrium between the ocean and the atmosphere is observed in large regions of the present oceans (32). Deeper vertical mixing or upwelling is a possible mechanism to explain the higher surface-water $[\text{CO}_{2(aq)}]$. The depth profile of $[\text{CO}_{2(aq)}]$ in a nearby Geochemical Ocean Sections Study (GEOSECS) station reveals that the calculated glacial-Holocene difference is equivalent to the variation of $[\text{CO}_{2(aq)}]$ within the upper 100 m in the modern Southern Ocean. The GEOSECS data also indicate that the deep mixing will cause a depletion in the *N. pachyderma* $\delta^{13}\text{C}$, but the expected change [0.4 to 0.5 per mil (33)] is smaller than that observed in our data and that from a much larger set

of *N. pachyderma* records in the Southern Ocean (24). The glacial $[\text{CO}_{2(aq)}]$ increase does not provide a simple way to explain the observed $\delta^{15}\text{N}$ records.

Our data imply that productivity was lower in the southern Atlantic during the glacial period than during the Holocene. Mechanisms proposed for the regulation of atmospheric CO_2 through changes in the high-latitude biological pump efficiency must therefore be reevaluated. Researchers must either look for different oceanic sectors with high glacial productivity or for alternative mechanisms that do not involve the biological pump. The relative contributions of changes in productivity and in surface seawater $[\text{CO}_{2(aq)}]$ to the production of the observed isotopic signals are uncertain. However, the effect of $[\text{CO}_{2(aq)}]$ appears to predominate in the present ocean (31). The two mechanisms are not mutually exclusive, and a combination of the two is possible if some factor other than nutrient availability limited diatom productivity during the LGM, such as ice persisting into the growing season or the stability of the mixed layer. However, reduced LGM productivity can account for all the variations observed in the three isotopic tracers.

REFERENCES AND NOTES

1. W. Berner, H. Oeschger, B. Stauffer, *Radiocarbon* 22, 227 (1980).
2. J. M. Barnola, D. Raynaud, Y. S. Korotkevich, C. Lorius, *Nature* 329, 408 (1987).
3. A. Neftel, H. Oeschger, T. Staffelbach, B. Stauffer, *ibid.* 331, 609 (1988).
4. W. H. Berger and R. S. Keir, *Geophys. Monogr. Am. Geophys. Union* 29, 337 (1984).
5. W. S. Broecker, *Geochim. Cosmochim. Acta* 46, 1689 (1982).
6. ———, *Global Biogeochem. Cycles* 3, 215 (1989).
7. J. L. Sarmiento and J. R. Toggweiler, *Nature* 308, 621 (1984).
8. U. Siegenthaler and T. Wenk, *ibid.*, p. 624.
9. F. Knox and M. B. McElroy, *J. Geophys. Res.* 89, 4629 (1984).
10. L. D. Labeyrie and J.-C. Duplessy, *Palaeogeogr. Palaeoclimatol. Palaeoecol.* 50, 217 (1985).
11. E. A. Boyle, *Paleoceanography* 3, 471 (1988).
12. P. N. Froelich, R. A. Mortlock, A. Shemesh, *Global Biogeochem. Cycles* 3, 79 (1989).
13. R. A. Mortlock *et al.*, *Nature* 351, 220 (1991).
14. N. Kumar, R. Gwiazda, R. F. Anderson, P. N. Froelich, *ibid.* 362, 45 (1993).
15. R. Francois, M. A. Altabet, L. H. Burckle, *Paleoceanography* 7, 589 (1992).
16. The value of $\delta^{13}\text{C} = (R_{\text{sample}}/R_{\text{standard}} - 1)1000$, where $R = ^{13}\text{C}/^{12}\text{C}$; $\delta^{15}\text{N} = (R_{\text{sample}}/R_{\text{standard}} - 1)1000$, where $R = ^{15}\text{N}/^{14}\text{N}$.
17. G. H. Rau, P. N. Froelich, T. Takahasi, D. J. Des Marais, *Paleoceanography* 6, 335 (1991).
18. K. H. Freeman and J. M. Hayes, *Global Biogeochem. Cycles* 6, 185 (1992).
19. J. P. Jasper and J. M. Hayes, *Nature* 347, 462 (1990).
20. G. H. Rau *et al.*, *Geochim. Cosmochim. Acta* 56, 1413 (1992).
21. G. D. Farquhar, M. H. O'Leary, J. A. Berry, *Aust. J. Plant Physiol.* 9, 121 (1982).
22. S. A. Macko *et al.*, *Chem. Geol. Isot. Geosci. Sect.* 65, 79 (1987).
23. M. A. Altabet, W. G. Deuser, S. Honjo, C. Stienen, *Nature* 354, 136 (1991).
24. C. D. Charles and R. G. Fairbanks, in *Geological*

History of the Polar Oceans: Arctic Versus Antarctic, U. Bleil and J. Theide, Eds. (Kluwer, Dordrecht, the Netherlands, 1990), pp. 519–538.

25. A. Shemesh, R. A. Mortlock, P. N. Froelich, *Paleoceanography* 4, 221 (1989).
26. A. Shemesh, C. D. Charles, R. G. Fairbanks, *Science* 256, 1434 (1992).
27. We analyzed $\delta^{13}\text{C}_{\text{org}}$ and $\delta^{15}\text{N}$ of purified diatoms with diameters $<38\ \mu\text{m}$. Combustion took place in quartz tubes at 850°C by standard techniques, and the overall reproducibility for diatom samples was 0.16 and 0.2 per mil for carbon and nitrogen, respectively. Amino acids were extracted by dialysis after cold hydrofluoric acid dissolution and analyzed in the soluble and insoluble fractions.
28. D. M. Swift and A. P. Wheeler, *J. Phycol.* 28, 202 (1992).
29. H. A. Lowenstam and S. Weiner, *On Biomineralization* (Oxford Univ. Press, New York, 1989).
30. W. M. Sackett, *Org. Geochem.* 9, 63 (1986).
31. G. H. Rau, in *Carbon Cycling in the Global Ocean:*

- Constraints on the Ocean's Role in Global Climate Change*, R. Zahn, M. Kaminski, L. D. Labeyrie, T. F. Pederson, Eds. (NATO Advanced Scientific Instrumentation Series, Springer, Berlin, in press).
32. P. P. Tans, I. Y. Fung, T. Takahashi, *Science* 247, 1431 (1990).
 33. P. Kroopnick, *Deep Sea Res.* 32, 57 (1985).
 34. J. D. Hays, J. A. Lozano, N. J. Shackleton, G. Irving, *Geol. Soc. Am. Mem.* 145, 337 (1976).
 35. We thank R. Edelman and A. Singer for laboratory assistance and two reviewers for helpful comments. Supported by grants from the U.S.-Israel Binational Science Foundation and the Faivovich Foundation (A.S.), National Science Foundation and National Oceanic and Atmospheric Administration grants (G.H.R.), and contribution 94 from the Department of Environmental Sciences and Energy Research, Weizmann Institute of Science.

5 May 1993; accepted 16 August 1993

A 5000-Year Record of Extreme Floods and Climate Change in the Southwestern United States

Lisa L. Ely,* Yehouda Enzel, Victor R. Baker, Daniel R. Cayan

A 5000-year regional paleoflood chronology, based on flood deposits from 19 rivers in Arizona and Utah, reveals that the largest floods in the region cluster into distinct time intervals that coincide with periods of cool, moist climate and frequent El Niño events. The floods were most numerous from 4800 to 3600 years before present (B.P.), around 1000 years B.P., and after 500 years B.P., but decreased markedly from 3600 to 2200 and 800 to 600 years B.P. Analogous modern floods are associated with a specific set of anomalous atmospheric circulation conditions that were probably more prevalent during past flood epochs.

Changes in the character of extreme events are likely to constitute a greater portion of the impact of climate change than slow alterations in mean conditions (1–3). Yet, even the longest available instrumental hydrological records inadequately represent rare, severe floods, which are commonly assumed to occur randomly in time for convenience in hazard assessment (4). Simulations with general circulation models have indicated that widespread increases in rainfall intensity and floods could be a consequence of climatic changes under increased atmospheric CO_2 (2), but an initial understanding of the full range and causes of natural variability in the existing hydrological system is essential to the forecasting and evaluation of the possible nature of these extreme events in the future. Geological evidence of ancient floods reveals that the magnitude and frequency of the largest floods vary with changing climatic condi-

tions on time scales of centuries to millennia (3, 5). We combined analyses of a 5000-year paleoflood record and modern flood analogs to investigate the specific relation between extreme floods and broad-scale atmospheric circulation patterns, providing a basis for the incorporation of this hydrological response into climate simulations.

This study summarizes depositional evidence of 251 paleofloods on 19 rivers in Arizona and southern Utah (Fig. 1) (5, 6). During floods in stable bedrock river channels, fine-grained sediments settle out of suspension in eddies or backwater zones where the flow velocity is diminished (7). This setting selectively preserves a complete catalog of the largest floods, which tend to leave a sequence of high deposits in protected niches away from the main flow of the river (8). Lower inset deposits from smaller floods are more susceptible to subsequent erosion (5). Each site in this study contained deposits from several floods, the ages of which were determined from occasional cultural artifacts and over 150 radiocarbon (^{14}C) dates on incorporated organic materials (5, 7, 9). Correlative paleoflood chronologies from different sites along a river reach were consolidated into one.

Combination of the records from several rivers in the region highlights clustering in

the frequency of large floods that is not detectable from a single river alone. The regional chronology (Fig. 2) shows distinct variations in the frequency of large floods over the last 5000 years. Periods of numerous large floods span 5 to 3.6 thousand ^{14}C years ago (ka) (3800 to 2200 B.C.), 2.2 to 0.8 ka (400 B.C. to 1200 A.D.), and 0.6 ka (1400 A.D.) to present (10). Large floods are completely absent between 3.6 and 2.2 ka (2200 to 400 B.C.), a period unlike any other in the 5000-year record. A sharp drop in the number of large floods also occurs from 0.8 to 0.6 ka (1200 to 1400 A.D.), immediately after a brief episode of particularly frequent high-magnitude floods from 1.0 to 0.8 ka (1000 to 1200 A.D.).

The number of flood deposits after 0.6 ka exceeds the scale of the graph (Fig. 2). To compare this peak with the earlier flood periods, we omitted sites with less than 400 years of record and recent inset deposits that are not likely to be preserved and divided the number of floods in each 200-year interval by the number of rivers represented in that interval. A substantial increase in floods in the last 600 years was still apparent, especially in the last 200 to 400 years, evidence that this pattern is not merely an artifact of differential preservation (11).

The extended periods of numerous large floods coincide with cool regional and global temperatures, reflected in neoglaciation advances and vegetation changes (12–14). High lake levels before 3.6 ka and in the last 400 years also indicate wetter conditions in the Southwest during these periods (15, 16) (Fig. 2). The paleofloods provide the additional evidence of a concurrent increase in the frequency of extreme storms (17).

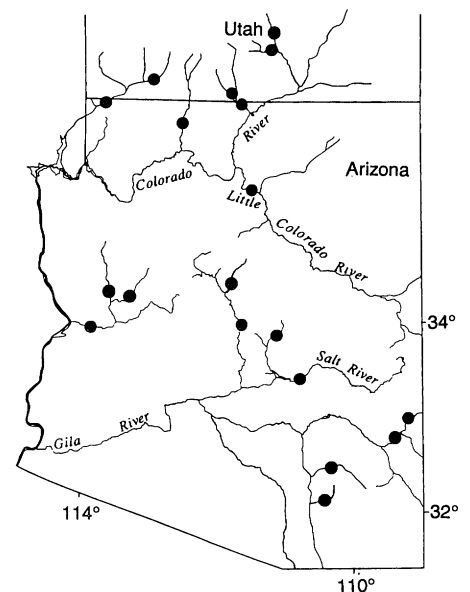


Fig. 1. Locations of flood deposit sites used in the regional paleoflood chronology (5, 6).

L. L. Ely, Earth System Science Center, Pennsylvania State University, University Park, PA 16802.

Y. Enzel, Institute of Earth Sciences, Hebrew University, Jerusalem 91904, Israel.

V. R. Baker, Department of Geosciences, University of Arizona, Tucson, AZ 85721.

D. R. Cayan, Climate Research Division, Scripps Institution of Oceanography A-024, University of California, La Jolla, CA 92093.

*To whom correspondence should be addressed.